# Quantifying and mitigating uncertainties in design optimization including off-the-shelf components: Application to an electric multirotor UAV

F. Pollet, M. Budinger, S. Delbecq, J.-M. Moschetta, J. Liscouët

# Quantifying and mitigating uncertainties in design optimization including off-the-shelf components: application to an electric multirotor UAV

F. Pollet[a,*], M. Budinger[b], S. Delbecq[a], J-M. Moschetta[a], J. Liscouët[c]

[a] *ISAE-SUPAERO, Université de Toulouse, 10 Avenue Edouard Belin, 31400 Toulouse, France*
[b] *ICA, Université de Toulouse, UPS, INSA, ISAE-SUPAERO, MINES-ALBI, CNRS, 3 rue Caroline Aigle, 31400 Toulouse, France*
[c] *Concordia University, 1455 De Maisonneuve Blvd., Montreal, QC H3G 1M8, Canada*

**Abstract**

This article proposes an approach to quantify and manage uncertainty in the conceptual design of aerial vehicles. A growing number of aerial vehicles, such as unmanned aerial vehicles (UAVs), are being wholly or partly designed with off-the-shelf components to streamline development and certification costs. The design optimization of systems typically relies on component design models in the continuous domain. In addition to the inaccuracies in the design models, the continuous domain condition is inconsistent with the finite number of components available in the market. This inconsistency yields uncertainty about the actual characteristics of the components defined by the continuous design process, hence inaccurate performance predictions at the system's level. The proposed approach is developed within the scope of the conceptual design of multirotor UAVs and covers the uncertainties

*Corresponding author (+33 5 61 33 85 35)
*Email address:* felix.pollet@isae-supaero.fr (F. Pollet)

related to both the design models and off-the-shelf components availability. Simple criteria are established to determine the importance of uncertainties according to the density of products in an off-the-shelf component database. The uncertainties are propagated through the system's models to evaluate the variance of the outputs and identify the most critical design parameters. A multidisciplinary design optimization framework enabling custom, off-the-shelf, and hybrid design is introduced and illustrated with a multirotor UAV case study. This case study demonstrates that switching from a custom design to an off-the-shelf selection for the most critical component, namely the propeller, results in a 69% reduction in the standard deviation of estimated hover endurance. The results obtained demonstrate that the proposed approach can contribute to the emergence of future aerial vehicles and systems that must meet demanding economic and performance targets by combining custom and off-the-shelf components in their design.
*Keywords:* Uncertainty Modelling, Uncertainty Analysis, Multidisciplinary Design Optimization, Off-The-Shelf Components, Hybrid Design Optimization, Unmanned Aerial Vehicles

---

**Nomenclature**

$MDO$ Multidisciplinary Design Optimization

$PCA$ Principal Component Analysis

$UAV$ Unmanned Aerial Vehicle

$XDSM$ Extended Design Structure Matrix

## 1. Introduction

Recent years have seen the development of numerous design optimization frameworks for sizing aerial vehicles [1]. Existing approaches typically parameterize the key components of the system with mathematical models and solve the optimization problem in the continuous domain [2, 3, 4, 5, 6, 7]. This strategy yields critical issues in the context of conceptual design. Firstly, the models employed in the conceptual design phase are often associated with large uncertainty because of their low fidelity. Secondly, designers are increasingly focusing on the integration of off-the-shelf components instead of custom-made parts to improve development times and production costs. A priori, this approach, which constrains the selection to a finite number of components, is inconsistent with a continuous-domain optimization. This inconsistency leads to some uncertainty about the actual characteristics of discretely available components as opposed to the custom definition provided by the conceptual design process in the continuous-domain.

Although the effects of uncertainty in the conceptual design of aircraft have been addressed in previous studies [8, 9, 10, 11, 12, 13], none of this previous work covers the uncertainties of transitioning from a continuous design space to a finite set of solutions (i.e., a discrete design space). In addition, many studies address uncertainty in design optimization through robust design [14], and the main trend for uncertainty reduction is to increase the fidelity level of the models for better prediction [15]. Yet, none of these approaches address the uncertainty about the market availability of the components specified by the design.

Reducing uncertainty requires transitioning from a pure continuous-domain

optimization to a hybrid continuous and discrete optimization, enabling custom definition and selection of off-the-shelf components from a database. Various methodologies explore databases to find the appropriate components [16, 17, 18, 19, 20, 21, 22, 23]. The most straightforward method consists of an exhaustive evaluation of all combinations of components from a database. Although some authors have proposed filtering operations to speed up the process [16], this technique remains computationally very costly because of the combinatorial explosion. Other approaches rely on advanced algorithms to solve the discrete optimization problem [24]. Magnussen [17, 18] introduced a framework for the design optimization of multirotors with off-the-shelf components. As in [19], the optimal solution is obtained with a mixed-integer linear program solver. However, the number of boolean design variables is proportional to the number of products in the database (up to 3091 variables in Magnussen's case study), making it impractical for complex problems. Ng [20] and Arellano-Quintana [21] use genetic algorithms to find the best combination of components. Discrete-integer design variables representing the indices of the selected components are introduced to solve the optimization problem. Consequently, the bounds on the design variables are equal to the number of components stored in the database, and the problem formulation is bonded to the latter. An alternative approach consists of solving the problem in the continuous domain and using the solution as a reference to find the closest components in a database [22, 23]. Because of the offline discretization process, this two-step method breaks the inter-dependencies between the components, and no feedback on the design is performed to verify the constraint satisfaction and optimality of the discrete solution. As a consequence,

no design methodology in the literature optimizes the design of systems with off-the-shelf components in an efficient manner. Furthermore, no existing approach allows choosing which components should be selected off-the-shelf and which should be parameterized using models without reformulating the optimization problem.

To address the above knowledge gaps and challenges, this paper introduces a methodology for evaluating and mitigating uncertainties in the context of design optimization, with a focus on the uncertainty driven by the discrete availability of components optimally sized in a continuous domain. The methodological framework is described in Section 2. The major sources of uncertainty at the conceptual design stage are characterized and quantified in Section 3. Methods for propagating uncertainties through a system's model and for ranking their importance are proposed in Section 4. These methods are then applied through a case study of a multirotor UAV. Section 5 introduces a methodology for the design optimization of systems, including both custom and off-the-shelf components, and compares three designs of multirotor UAVs with different levels of uncertainty. Finally, Section 6 concludes this paper.

## 2. Methodological framework for uncertainty assessment and mitigation

The modelling of uncertainties and their propagation through a physical model has been covered in previous works [25, 26, 27, 28]. In this section, the methodological principles are extended to the detailed treatment of uncertainties and their reduction. The proposed methodological framework for

quantitative uncertainty assessment and mitigation consists of four steps:

1. Identify and model the system. The model generally consists of one or several deterministic functions $\underline{y} = F(\underline{x}, \underline{\theta})$ linking a set of inputs $\underline{x}$ to a set of outputs $\underline{y}$ through equations involving specific model parameters $\underline{\theta}$. In this article, a pre-existing model describing the propulsion system for electric multirotor UAVs with several sub-models $f_i$ is considered [29].
2. Quantify and characterize the sources of uncertainty. The system model may be affected by a great variety of uncertain variables resulting from a lack of data, measurement errors, or aleatory phenomena. Section 3 covers the probabilistic description of uncertainties arising from incomplete knowledge, including model errors and uncertain values for the model inputs.
3. Propagate uncertainties through the system model to get a measure of uncertainty in the output variables of interest. In this study, the Monte Carlo method is performed to obtain the probabilistic distributions of the outputs. A screening method is applied as a preliminary analysis for reducing the number of uncertain variables prior to the Monte Carlo simulations. This approach is described in Section 4.
4. Perform a sensitivity analysis to assess the relative importance of uncertainties. This step aims at analyzing which parameters are the most important in determining the variability in the outputs of interest. Section 4 provides an analytical method and a more advanced variance-based method for importance ranking.
5. Mitigate uncertainties. In this article, the focus is on removing impor-

tant sources of uncertainty arising from the unknown availability of the components defined in a continuous design space. In contrast, selecting a component directly from a database provides better knowledge of its parameters. For this purpose, Section 5 introduces a versatile methodology for the design optimization of systems, including either custom or off-the-shelf components.

The five steps described in this process can be repeated until the level of uncertainty is deemed acceptable.

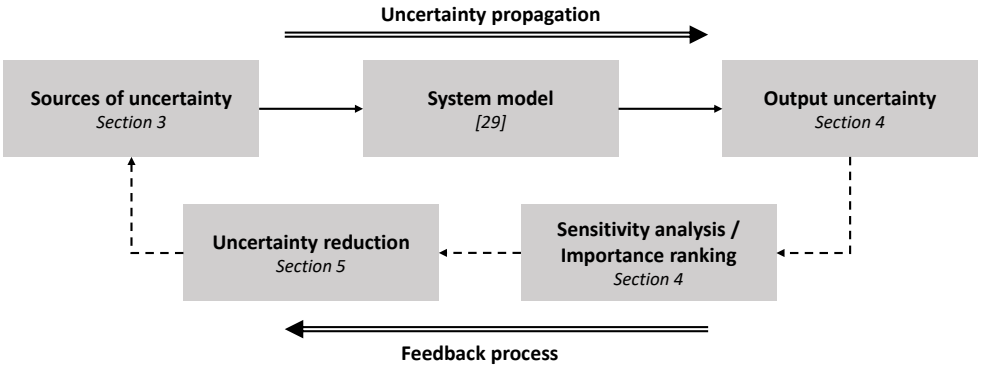


Figure 1: Methodological framework for uncertainty assessment (adapted from [26, 28]).

## 3. Sources of uncertainty

The sources of uncertainty can be either aleatory (irreducible) or epistemic (reducible) [27, 28, 26]. Aleatory uncertainty concerns unpredictable variations inherent to physical systems and their environments, and as such, cannot be controlled. The amplitude of the gusts that an aircraft will encounter in its lifetime is an example of such uncertainty. In contrast, epistemic uncertainty originates from a lack of knowledge of the system. Epis-

temic uncertainty can be reduced by an increase in available data, such as measures or experts' knowledge. The focus of this paper is on epistemic uncertainty, for which we propose the following classification:

- *Model uncertainty* relates to the accuracy with which a model reflects reality. Model uncertainty includes, among others, the inadequate structure of the model, low numerical resolution, and erroneous fitting of the model parameters. In this paper, all sources of model uncertainty are considered without distinction in the model parameters.

- *Input uncertainty* is associated with the input design variables of a model. In the context of conceptual and preliminary design, design models are used to estimate the functional parameters of the components from a few design variables. For instance, the resistance of an electric motor may be estimated from its nominal torque and velocity constant. Input uncertainty relates to the level of information available on the input design variables, which varies according to the design stage. It is reduced to zero after all design variables have been determined, that is, when the component selection is finalized.

Model uncertainty acts on the model parameters $\underline{\theta}$, while input uncertainty affects the input variables $\underline{x}$. Consequently, the uncertainties on the outputs $\underline{y} = F(\underline{x}, \underline{\theta})$ arise from both model uncertainty and input uncertainty.

In the following sections, a pre-existing model describing the propulsion system of multirotor UAVs is introduced, and the model and input uncertainties are characterized. The focus is on the design models introduced by Budinger et al. in [29] for estimating the properties of the key components of

the electric propulsion system. The main scaling laws and regression models for sizing the propellers, motors, batteries, and electronic speed controllers (ESC) are reused here and recalled in Table 1.

Table 1: Models for the preliminary design of multirotor UAVs [29].

| | Output variable $y$ | Model equation | Model parameters $\theta$ | Input variables $x$ |
|---|---|---|---|---|
| Propeller | Mass $M$ [kg] | $M = \theta_1 D^3$ | $\theta_1 = \frac{M_{ref}}{D_{ref}^3}$ | Diameter $D$ [m] |
| | Thrust coefficient $C_T$ [-] | $C_T = \theta_2 + \theta_3 \beta$ | $\theta_2 = 4.27 \times 10^{-2}$ | Pitch-to-diameter $\beta$ [-] |
| | | | $\theta_3 = 1.44 \times 10^{-1}$ | |
| | Power coefficient $C_P$ [-] | $C_P = \theta_4 + \theta_5 \beta$ | $\theta_4 = -1.48 \times 10^{-3}$ | Pitch-to-diameter $\beta$ [-] |
| | | | $\theta_5 = 9.72 \times 10^{-2}$ | |
| Motor | Mass $M$ [kg] | $M = \theta_6 T_{nom}$ | $\theta_6 = \frac{M_{ref}}{T_{nom,ref}}$ | Nominal torque $T_{nom}$ [N.m] |
| | Resistance $R$ [$\Omega$] | $R = \theta_7 K_V^{-2} T_{nom}^{-5/3.5}$ | $\theta_7 = \frac{R_{ref}}{K_{V,ref}^{-2} T_{nom,ref}^{-5/3.5}}$ | Velocity constant $K_V$ [rad/V/s] |
| | | | | Nominal torque $T_{nom}$ [N.m] |
| | Friction torque $T_f$ [N.m] | $T_f = \theta_8 T_{nom}^{0.69}$ | $\theta_8 = \frac{T_{f,ref}}{T_{nom,ref}^{0.69}}$ | Nominal torque $T_{nom}$ [N.m] |
| ESC | Mass $M$ [kg] | $M = \theta_9 P$ | $\theta_9 = \frac{M_{ref}}{P_{ref}}$ | Power $P$ [W] |
| Battery | Mass $M$ [kg] | $M = \theta_{10} E$ | $\theta_{10} = \frac{M_{ref}}{E_{ref}}$ | Energy $E$ [Wh] |

*Subscript $_{.ref}$ refers to reference components used for fitting the models.*

### *3.1. Model uncertainty*

The scaling laws and regression models introduced by Budinger [29] require a limited number of input variables and, as such, are well suited for preliminary design. However, several simplifying assumptions had to be made to obtain the models. Geometric similarity assumes constant length ratios between the sized components and the reference components used for fitting the models. This similarity assumption is also applied to the material properties. Finally, the uniqueness of the design driver states that only one dominant physical phenomenon drives the evolution of the characteristic to be estimated. When these assumptions are not satisfied, the accuracy of the

model deteriorates, and model uncertainty arises. The estimated value of the output, $\hat{y}$, deviates from the true value $y$:

$$y = (1 + \varepsilon_\theta)\hat{y} = (1 + \varepsilon_\theta) f(x, \theta^*), \tag{1}$$

where $\varepsilon_\theta$ is the relative error and $f(x, \theta^*)$ is the model equation whose parameter $\theta^*$ is obtained with appropriate fitting methods (e.g., error minimization). Since the models presented in Table 1 are linear with respect to their parameters $\theta_i^*$, it follows that

$$y = f\left(x, (1 + \varepsilon_\theta)\theta^*\right) = f(x, \theta), \tag{2}$$

with $\theta = (1 + \varepsilon_\theta)\theta^*$. The inaccuracies of the models are described by deviations in the model parameters, that is, model uncertainties. The model uncertainties of scaling laws and regressions are modelled as independent normal laws [29]:

$$\varepsilon_\theta \sim \mathcal{N}(\mu_\theta, \sigma_\theta^2) \tag{3}$$

$$\Leftrightarrow \ \theta \sim \Theta = \mathcal{N}\left((1 + \mu_\theta)\theta^*, \sigma_\theta^2 \theta^{*2}\right) \tag{4}$$

The mean $\mu_\theta$ and standard deviation $\sigma_\theta$ of the normal distributions are mainly influenced by the choice of the reference components for fitting the equations and the form of the equations since uncertainty increases with higher order terms. Figure 2 shows the distribution of the relative error for the estimated battery mass, and its comparison to a normal distribution.

### *3.2. Input uncertainty*

Uncertainty about the design variables of the components (i.e., the inputs of the design models) may arise from various sources. In particular, the

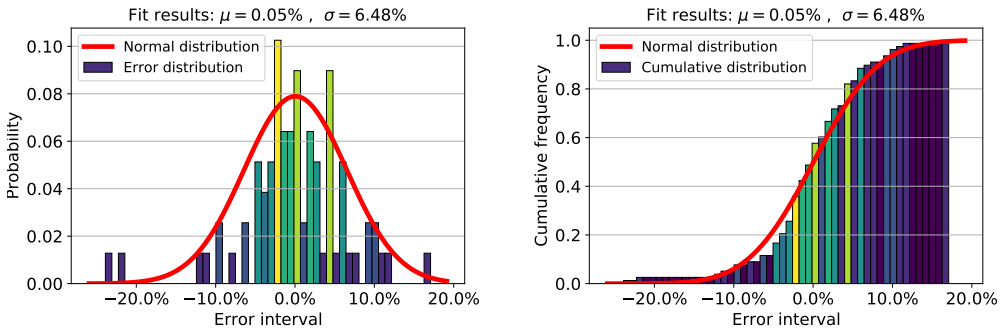


(a) Probability distribution

(b) Cumulative distribution

Figure 2: Relative error distribution for the estimated battery mass [29].

impossibility of guaranteeing a component's availability on the market is a major source of uncertainty at the early stages of the design process. Indeed, manufacturers limit their production to specific ranges of components for economic reasons. Thus, during the design process, a gap exists between the optimal characteristics of a component that would be custom-made and the characteristics of the closest off-the-shelf component available. If the catalogs of components are not known a priori by the designer, for instance, at the conceptual design stage, the latter faces uncertainty on the values of the input variables to be used for the models (e.g., propeller diameter). This section describes the input uncertainty associated with an incomplete market offer.

In [30], Pahl et al. suggest that manufacturers follow a size range approach when designing their products by limiting their production to a few selected sizes in order to reduce costs. A standardized methodology is often adopted by manufacturers to determine the best distribution of components, i.e. choosing an optimal size range while best meeting consumer demand.

Starting from an initial design, new designs are derived, which are arranged in a mathematical sequence. While an arithmetic progression on a design variable's value is straightforward, Pahl et al. advise choosing these quantities according to a geometric progression within a range. Whether an arithmetic progression or geometric progression approach is adopted depends on the market.

The arithmetic progression approach consists of deriving the new designs with a constant increment on a parameter describing the component (e.g., propeller diameter). For the $n$-th component in the size range, the value $x_n$ of its parameter is obtained from an initial design $x_0$ as follows:

$$x_n = x_0 + nd, \tag{5}$$

with $d$ the increment step. When a customer selects a component from a catalogue, he chooses the component whose characteristics are nearest (or nearest upper, or nearest lower) to his specifications. The selection process is represented in Figures 3 and 4, where a continuous set of input values is mapped to a countable set, with a finite number of elements built on an arithmetic progression. The associated absolute error between the continuous variable $x^*$ and the discrete variable $x$ is plotted in Figure 4.

The absolute error has a uniform distribution bounded by half the increment step:

$$\eta_x = x - x^* \sim \mathcal{U}\left(-\frac{d}{2}, \frac{d}{2}\right) \tag{6}$$

$$\Leftrightarrow \; x \sim X = \mathcal{U}\left(x^* - \frac{d}{2}, x^* + \frac{d}{2}\right) \tag{7}$$

Hence, a denser database yields less uncertainty. The APC multirotor propellers [31] provide an example of arithmetic scaling on the diameter.

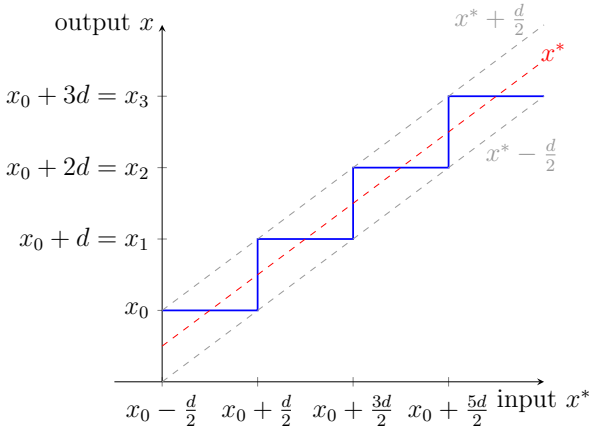


Figure 3: Arithmetic progression mapping.

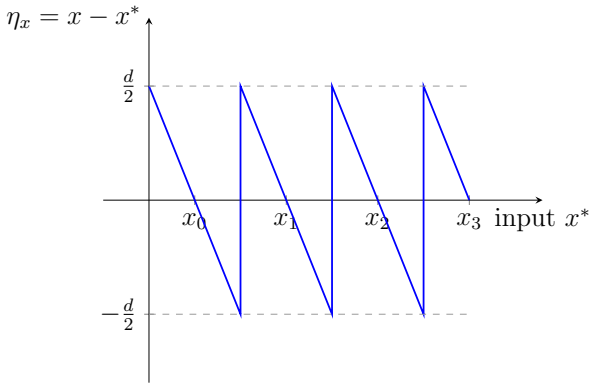


Figure 4: Absolute error of the arithmetic progression mapping.

The size range covers diameters from 0.153 to 0.406 meters, with an average difference $d$ of 0.0254 meters, that is, exactly one inch. Figure 5 depicts the absolute error distribution of the diameter and its comparison with a uniform distribution law.

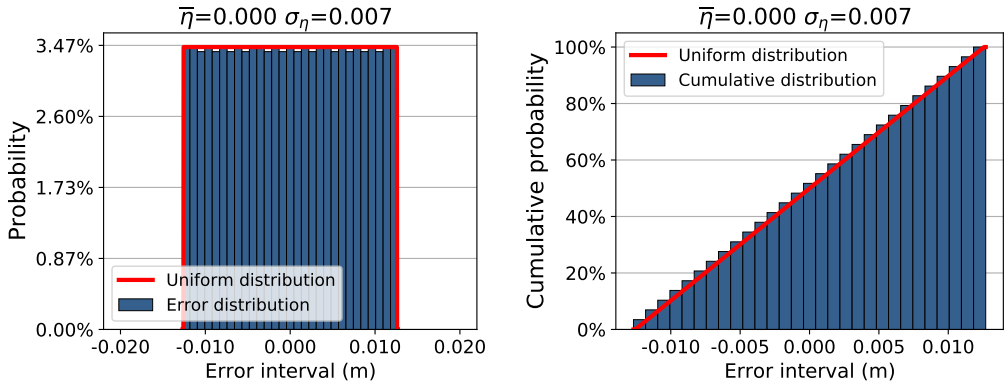


(a) Probability distribution

(b) Cumulative distribution

Figure 5: Absolute error distribution of the propeller diameter and comparison to a uniform distribution.

For other components available on the market, a geometric progression might be more representative [30]. It consists of multiplying the value of a parameter describing the component by a constant ratio $r$ in order to derive the new designs:

$$x_n = x_{n-1}r = x_{n-2}r^2 = ... = x_0 r^n, \tag{8}$$

The mapping for a size range built on a geometric progression is represented in Figures 6 and 7. The magnitude of the absolute error $\eta_x$ between the continuous variable and the real variable is significantly correlated to the magnitude of the input. A probabilistic description would hide this behavior

and is therefore not desirable. Instead, a probabilistic model of the relative error $\varepsilon_x$ is adopted, as its magnitude is not correlated with the input. The relative error distribution follows a uniform law:

$$\varepsilon_x = \frac{x - x^*}{x^*} \sim \mathcal{U}(-\delta, \delta) \tag{9}$$

$$\Leftrightarrow \quad X = \mathcal{U}\left(x^*(1-\delta), x^*(1+\delta)\right), \tag{10}$$

with $\delta = \frac{r-1}{r+1}$. Here again, a high number of components within a size range (i.e., $r \to 1$) reduces the variable's uncertainty.

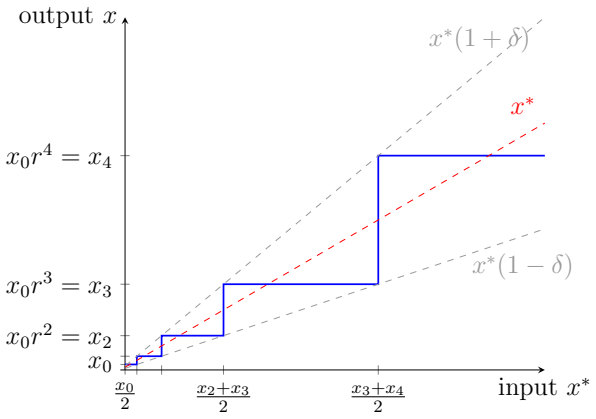


Figure 6: Geometric progression mapping.

A quasi-geometric scaling of the nominal motor torque is observed on a family of 15 ABB products [32] over the range 1-200 (N·m). The relative error falls between -17% and 17% with a uniform probability distribution.

If multiple design variables are involved in the selection process of a component, the random variables describing the uncertainties are assumed to be mutually independent, although this is not always verified in practice. Further work should focus on analyzing the interactions between various design variables describing a component.

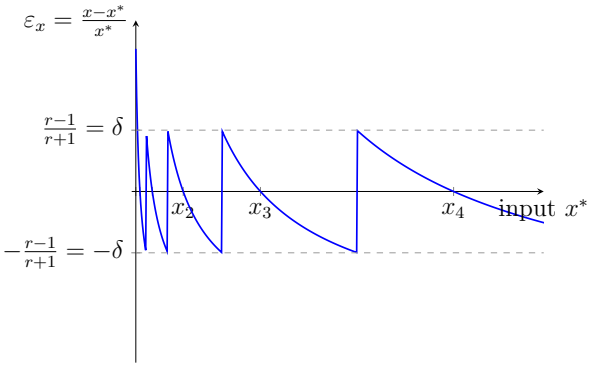


Figure 7: Relative error of the geometric progression mapping.

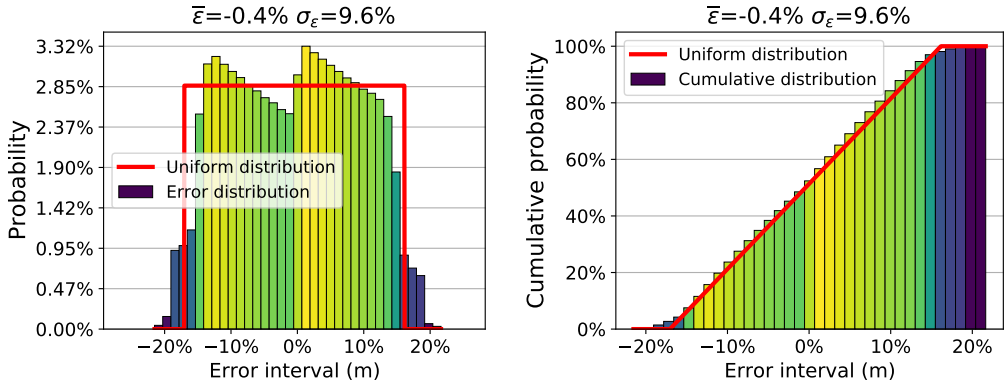


(a) Probability distribution

(b) Cumulative distribution

Figure 8: Relative error distribution of the nominal motor torque and comparison to a uniform distribution.

## 4. Uncertainty propagation and sensitivity analysis

### *4.1. Uncertainty propagation*

The previous sections have introduced the characterization and quantification of two sources of uncertainty. The uncertain input variables $x$ and model parameters $\theta$ can be modelled as random variables denoted $X$ and $\Theta$, respectively. Given the uncertainties on the set of input variables and model parameters describing a system, the next step is to obtain a characterization of the outputs distributions:

$$\underline{Y} = F(\underline{X}, \underline{\Theta}) \tag{11}$$

Here, the system model $F$ is made of several sub-models $f_i$ characterizing each element of the system. When the sub-models are interdependent, it can be difficult to derive the distributions of the system outputs analytically. Indeed, uncertainties propagate through the models and combine with each other. To overcome this difficulty, a Monte-Carlo method is adopted. It consists in evaluating the deterministic system model for many realizations of $\underline{X}$ and $\underline{\Theta}$ and observing the values taken by the outputs $\underline{Y}$. When a large number of realizations is achieved, the random variables associated with the outputs can be identified from the samples.

### *4.2. Sensitivity analysis*

Sensitivity analysis is the study of how uncertainty in a model output can be attributed to different sources. It aims at identifying the parameters that most influence the output, thus helping to determine the focus for future uncertainty mitigation.

A first approach for ranking uncertainties consists of analyzing the form of the equations involved in the modelling. Let suppose a model $f$ with uncertain input $x = (1+\varepsilon_x)x^*$ and uncertain model parameter $\theta = (1+\varepsilon_\theta)\theta^*$. A first-order approximation with Taylor series expansion at $(x^*, \theta^*)$ for small relative deviations $\varepsilon_x$ and $\varepsilon_\theta$ provides:

$$\begin{aligned} y &= f(x, \theta) \\ &= f(x^* + x^*\varepsilon_x, \theta^* + \theta^*\varepsilon_\theta) \\ &= f(x^*, \theta^*) + x^*\varepsilon_x \frac{\partial f}{\partial x}(x^*, \theta^*) + \theta^*\varepsilon_\theta \frac{\partial f}{\partial \theta}(x^*, \theta^*) + o(\sqrt{(x^*\varepsilon_x)^2 + (\theta^*\varepsilon_\theta)^2}) \end{aligned} \tag{12}$$

For power laws (e.g., scaling laws) in the form $f(x, \theta) = \theta x^a$, with $a$ the power law exponent, Equation 12 simplifies to:

$$y = f(x^*, \theta^*)(1 + a\varepsilon_x + \varepsilon_\theta) + o(\sqrt{(x^*\varepsilon_x)^2 + (\theta^*\varepsilon_\theta)^2}) \tag{13}$$

This allows for determining, with a first-order approximation, the variations of the output caused by input uncertainty and those caused by model uncertainty. The variances of their distributions are compared to assess the relative effects of the different sources of uncertainty. The variations of $y$ due to input uncertainty are considered equal to those due to model uncertainty if

$$|a|\, \sigma_x^2 = \sigma_\theta^2, \tag{14}$$

where $\sigma_x$ (resp., $\sigma_\theta$) is the standard deviation of the relative error $\varepsilon_x$ (resp., $\varepsilon_\theta$). For the input uncertainties with uniform distributions introduced in Section 3, the standard deviation $\sigma_x$ is linked to the constant step $d$ or

common ratio $r$ of the components' database:

$$\begin{cases} \sigma_x = \frac{d}{2\sqrt{3}} \frac{1}{|x^*|} & \text{for an arithmetic database} \\ \sigma_x = \frac{2\delta}{2\sqrt{3}} = \frac{1}{\sqrt{3}} \frac{r-1}{r+1} & \text{for a geometric database} \end{cases} \tag{15}$$

Equations 14 and 15 enable finding the assumption on database density (i.e., $d$ or $r$) such that the two sources of uncertainty have similar effects:

$$|a|\,\sigma_x^2 = \sigma_\theta^2 \Longleftrightarrow \begin{cases} d = \frac{2\sqrt{3}|x^*|\sigma_\theta}{\sqrt{|a|}} & \text{for an arithmetic database} \\ r = \frac{\sqrt{|a|}+\sigma_\theta\sqrt{3}}{\sqrt{|a|}-\sigma_\theta\sqrt{3}} & \text{for a geometric database} \end{cases} \tag{16}$$

This approach provides a rough estimate for ranking uncertainties when a single model is involved. For the models introduced in Section 3 Table 1, the outputs' variations due to model uncertainty are presented in Table 2. Estimates on the databases' densities such that the variations caused by input uncertainty match those caused by model uncertainty are presented in Table 3. For the motors database, a constant ratio $r = 1.50$ between two consecutive values of the nominal torque leads to equal effects of model and input uncertainty in the mass calculation. Considering a range within 1 - 10 N.m, there should be at least $\log_r(10/1) \approx 6$ products in the motor database for the input uncertainty to be secondary.

On more complex problems involving many equations, the use of numerical methods is often necessary. In this study, the Sobol' method [33, 34] is adopted to derive the global impact of uncertain parameters, taking into account the interactions between them. Based on a Monte-Carlo experiment, this method decomposes the variance of the output into terms of increasing dimensions, called sensitivity indices, that are attributed to the uncertain

Table 2: Outputs' variations caused by model uncertainty for the UAV models.

| | Output | Model uncertainty deviation $\sigma_\theta$ |
|---|---|---|
| Motor | Mass $M$ | 11.5% |
| | Resistance $R$ | 13.2% |
| | Friction torque $T_f$ | 33.4% |
| Battery | Mass $M$ | 7.1% |
| ESC | Mass $M$ | 25.4% |
| Propeller | Mass $M$ | 10.0% |
| | Thrust coefficient $C_T$ | 8.8% |
| | Power coefficient $C_P$ | 7.5% |

Table 3: Assumptions on databases' densities to match the variations caused by input uncertainty with those caused by model uncertainty.

| | Output | Input | Database progression such that $\lvert a \rvert \, \sigma_x^2 = \sigma_\theta^2$ | |
|---|---|---|---|---|
| Motor | Mass $M$ | Nominal torque $T_{nom}$ | Geometric | $r = 1.50$ |
| | Resistance $R$ | Velocity constant $K_V$ | Geometric | $r = 1.39$ |
| | | Nominal torque $T_{nom}$ | Geometric | $r = 1.47$ |
| | Friction torque $T_f$ | Nominal torque $T_{nom}$ | Geometric | $r = 5.59$ |
| Battery | Mass $M$ | Energy $E$ | Arithmetic | $d = 179.5$ Wh |
| ESC | Mass $M$ | Power $P$ | Arithmetic | $d = 782.7$ W |
| Propeller | Mass $M$ | Diameter $D$ | Arithmetic | $d = 0.098$ m |
| | Thrust coefficient $C_T$ | Pitch-to-diameter $\beta$ | Arithmetic | $d = 0.091$ |
| | Power coefficient $C_P$ | Pitch-to-diameter $\beta$ | Arithmetic | $d = 0.078$ |

parameters. The first-order indices measure the effect of varying a given input alone averaged over the variations of the other inputs [34]:

$$S_i = \frac{V_{X_i}\left(E_{X_{-i}}(Y|X_i)\right)}{V\left(Y\right)}. \tag{17}$$

Here, $E_{X_{-i}}(Y|X_i)$ denotes the average value of the output $Y$ when all inputs except $X_i$ vary, and $V_{X_i}\left(E_{X_{-i}}(Y|X_i)\right)$ is the variance of the previous quantity when $X_i$ varies. The variance of the output is denoted $V(Y)$. The second-order indices describe the coupled effect of two parameters on the output, and so on for higher-order indices. Finally, total-order effects [35] capture the contribution of an input by taking into account its interactions of any order with all other parameters [34]:

$$S_{T_i} = 1 - \frac{V_{X_{-i}}\left(E_{X_i}(Y|X_{-i})\right)}{V\left(Y\right)}. \tag{18}$$

Although variance-based methods provide accurate results, they require a large number of simulations to collect enough samples for calculating sensitivity indices. For $N$ uncertain inputs, the method of Sobol requires about $m \times (N+2)$ model evaluations, with $m$ ranging from hundreds to thousands.

To save time, the least-influential parameters can be removed beforehand with a screening study. Screening techniques such as the method of Morris [36] allow obtaining an estimate of the relative importance of uncertainty sources. The Morris method consists of calculating the partial derivative of the output function by varying the uncertain parameters one at a time. The process is repeated for different sets of start values for the other parameters, allowing the exploration of the entire domain of definition. The derivatives are then averaged out. Morris method provides two indicators: the mean effect $\mu^*$ of the input variation on the output and the standard deviation $\sigma$

that characterizes both non-linear effects and interactions with other sources of uncertainty. The Morris method requires $r \times (N + 1)$ model evaluations, where the number $r$ of different starting points typically ranges from 4 to 10 [37]. This efficient method is, therefore, an adequate tool to select only the most influential parameters prior to a thorough sensitivity analysis.

### *4.3. Case study: performance uncertainty of a multirotor UAV*

This section applies the methodology and tools for uncertainty assessment to study the flight performance of a multirotor UAV. The case study is the DJI M600 Pro hexacopter drone [38], whose main specifications are summarized in Table 4.

Table 4: Main specifications for the DJI M600 Pro [38].

| | |
|---|---|
| Number of propellers: | 6 |
| Payload: | 5.5 kg |
| Max thrust-to-weight ratio: | 2 |
| Max ascent speed: | 5 m/s |
| Hover endurance: | 18 min |

The sizing of the DJI M600 is retrieved by applying the analytical methodology previously developed by the authors [4, 39, 40]. This methodology applies a multidisciplinary design optimization (MDO) approach to efficiently size and optimize various UAV configurations. The multidisciplinary modelling covers the electric propulsion system (Table 1), the airframe, and the aerodynamics, among others. For conciseness and clarity, this study focuses on the uncertainty associated with the propulsion system, as introduced in

Section 3. The results of the analytical sizing and the comparison with the reference DJI M600 data are presented in Table 5. In what follows, the results of the analytical sizing will be considered as a deterministic reference for the uncertainty assessment.

Table 5: Results comparison for the analytical sizing of the DJI M600 Pro.

| | Reference [38] | Analytical sizing | Relative error (%) |
|---|---|---|---|
| Total mass (kg) | 15.5 | 15.4 | - 0.50 |
| Batteries mass (kg) | 4.08 | 3.82 | - 6.43 |
| Motors mass (kg) | 1.38 | 1.71 | + 24.12 |
| Propeller diameter (m) | 0.533 | 0.489 | - 8.31 |
| Battery energy (Wh) | 780 | 729 | - 6.43 |
| Motor max. power (W) | 1000 | 890 | - 11.04 |

*4.3.1. Probabilistic model and implementation*

The study focuses on 15 uncertain parameters of the propulsion system and their impact on hover flight endurance. The assumptions on the uncertain parameters are detailed in Appendix A. The probabilistic distributions are derived according to the methods introduced in Section 3. In particular, the uncertainties on the components' availability are estimated from catalogs of commercially available products[1]. Supplementary Material is provided in a Jupyter Notebook [44] for estimating input uncertainties from databases. In addition to input uncertainty and model uncertainty, some parameters ob-

[1]Manufacturers' catalogs: APC propellers for multirotors [31] (46 products), AXI motors [41] (52 products), ProLiteX batteries [42] (78 products), YGE ESC [43] (17 products)

tained from experts' judgments without specific models (e.g., the efficiency of the speed controller) are considered to be distributed uniformly within a range of values. Finally, the distributions are assumed to be mutually independent.

The statistical methods described in Section 4 are implemented using Python libraries. In particular, the Monte Carlo simulations and sensitivity analyses are performed using OpenTURNS [45] and SALib [46], respectively.

*4.3.2. Results and discussion*

As a preliminary analysis, the relative importance of model uncertainty and input uncertainty for each individual model is assessed from the form of the equations with the criteria derived in Equation 16. The calculations are made from the model uncertainties provided in [29] and the assumptions on the databases presented in Appendix A. The results are shown in Table 6. For each model of the propulsion system, the uncertainty arising from model discrepancy has more effect on the output than the uncertainty on the inputs. Thus, model uncertainties are expected to outweigh input uncertainties. However, this analysis does not allow for ranking the final effects of the sources of uncertainty on the hover flight endurance, as the scope is limited to each individual equation.

**Screening**

The screening method of Morris is applied to select a reduced set of uncertain parameters that most influence the hover endurance. The method is implemented with 10 different sets of start values, such that 160 calls to the complete UAV model are required. The results are shown in Figure 9. The most influential parameters are located in the upper-right quadrant of the

Table 6: Deviations caused by model uncertainty and input uncertainty within each model.

| | Output | Model uncertainty deviation $\sigma_\theta$ | Input uncertainty deviation $\sqrt{\lvert a \rvert}\sigma_x$ | |
|---|---|---|---|---|
| Motor | Mass $M$ | 11.5% | Nominal torque $T_{nom}$ | 3.6% |
| | Resistance $R$ | 13.2% | Velocity constant $K_V$ | 3.4% |
| | | | Nominal torque $T_{nom}$ | 4.3% |
| | Friction torque $T_f$ | 33.4% | Nominal torque $T_{nom}$ | 3.0% |
| Battery | Mass $M$ | 7.1% | Energy $E$ | 0.4% |
| ESC | Mass $M$ | 25.4% | Power $P$ | 10.2% |
| Propeller | Mass $M$ | 10.0% | Diameter $D$ | 2.7% |
| | Thrust coefficient $C_T$ | 8.8% | Pitch-to-diameter $\beta$ | 1.9% |
| | Power coefficient $C_P$ | 7.5% | Pitch-to-diameter $\beta$ | 1.9% |

$\sigma$ versus $\mu^*$ plot. It is observed that 3 parameters are highly important to explain the hover endurance: the propeller thrust coefficient $C_T$ and power coefficient $C_P$ obtained from a regression model, and the ESC efficiency. The model uncertainty on the battery mass, obtained from an assumed energy density, also has a significant impact on flight endurance. Furthermore, the model uncertainties of the motor resistance and motor mass have a great influence. The most influential uncertainties originate from discrepancies in the models rather than their inputs, which is consistent with the preliminary study presented in Table 6. This outcome reflects the high number of components available in the UAV market and should not be generalized to other systems. Finally, particular attention should be given to ESC efficiency, and the development of a specific model instead of an expertise-based value may

be relevant.

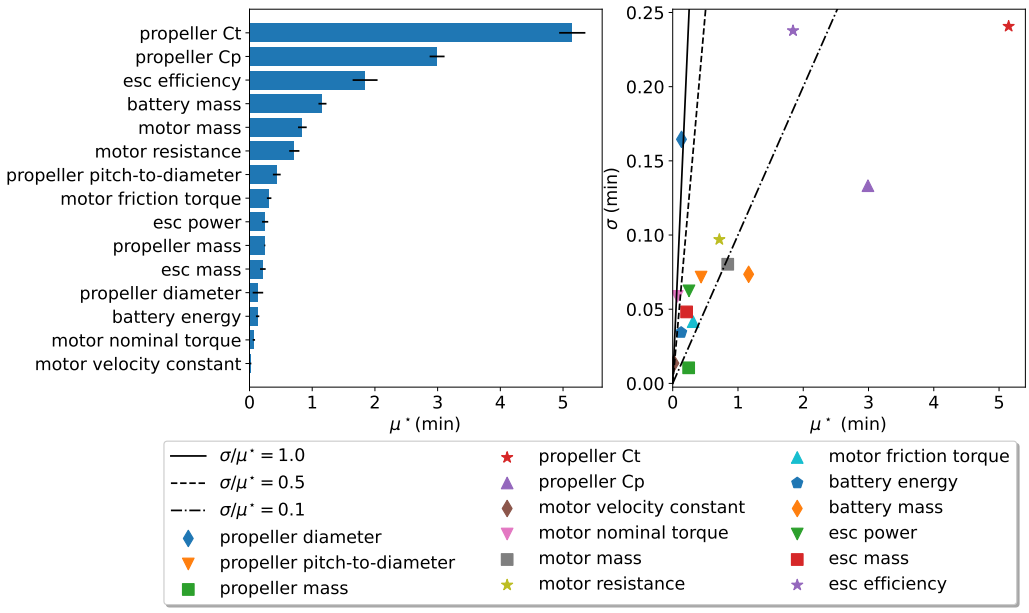


Figure 9: Screening results using Morris method

### Output distribution and sensitivity analysis

Propagation of uncertainty using Monte Carlo experiments is performed on the 7 most influential parameters identified with the method of Morris. This allows obtaining a distribution of the hover endurance. To achieve high precision in the output distribution, a high number of samples is required. Here, 1024 samples have been generated, which led to 9216 Monte Carlo simulations. The distribution of the flight endurance is shown in Figure 10. The observed distribution fits a normal law with a mean value $\mu = 18.1$ min and standard deviation value $\sigma = 3.2$ min.

The total- and first-order contributions to the output variance obtained with Sobol's method are given in Figure 11. The second and higher-order con-

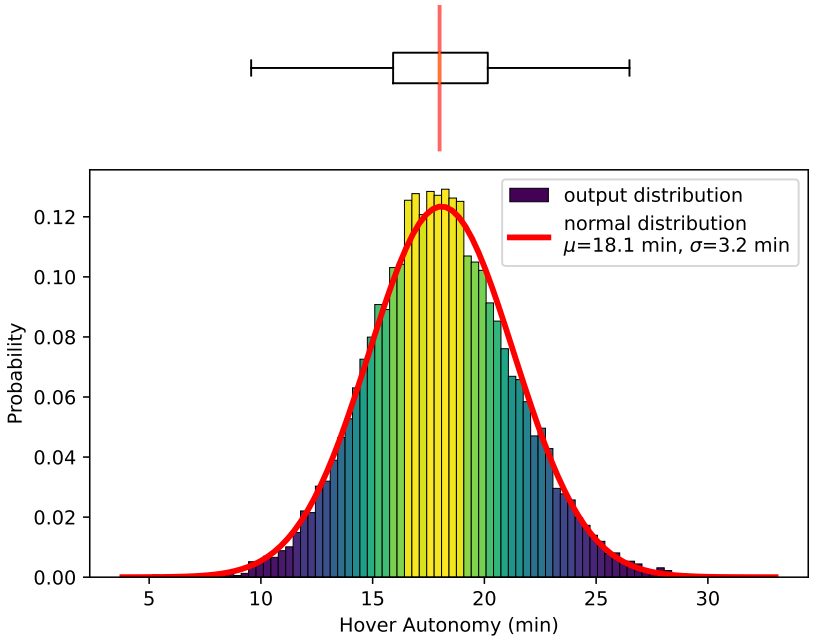


Figure 10: Distribution of the estimated hover endurance

tributions are close to zero, highlighting the negligible interactions between the pairs of parameters involved in the analysis. The standard deviations found in the Morris analysis are, therefore, more related to non-linearities in the models than interaction effects. A major conclusion of the sensitivity analysis is that the aerodynamic performance of the propellers significantly impacts flight endurance. This is because the mechanical power is obtained directly through the propeller performance. The variation in the component masses (e.g., battery mass) also affects the mechanical power, but the small variations of the estimated masses with respect to the total mass of the UAV limit their influence. The electrical power, which defines the flight endurance together with the battery energy, is calculated from the mechanical power and the efficiency of the electrical components (e.g., motor resistance and ESC efficiency). However, their importance is of second order. Finally, the sensitivity to the battery energy is negligible because of the large number of UAV batteries available on the market, hence the low uncertainty on this design variable.

## 5. Hybrid design optimization for uncertainty reduction

The previous sections have shown how uncertainty in various parameters affects the knowledge of the system's outputs of interest. In particular, there is a significant risk of overestimating the performance of the system. The actual design may, therefore, not be able to meet the performance requirements specified by the customer. The sensitivity analysis offers the possibility to identify the most influential sources of uncertainty so that actions can be taken to mitigate them. Among the possible actions, the designer can opt

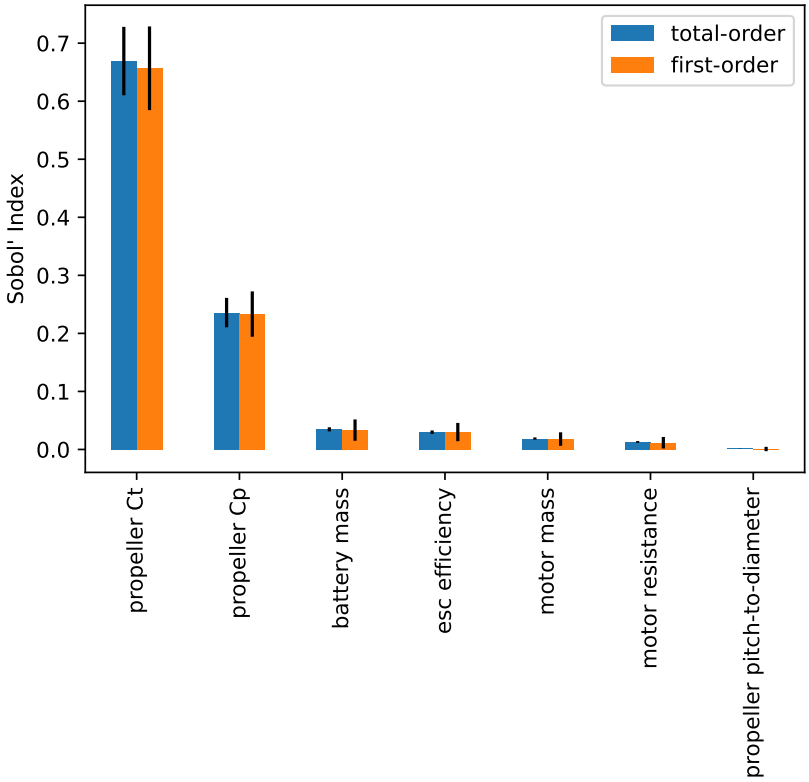


Figure 11: First- and total-order Sobol' indices

for increasing the fidelity of the models in order to improve their representativeness. Another common approach is to restrict the design space to a set of existing components listed in a database instead of parameterizing components with continuous models. Using off-the-shelf components whose parameters are listed in datasheets provides a deterministic description (Figure 13) in place of the probabilistic one associated with modelling of custom components (Figure 12). For example, the aerodynamic model of the propeller, which has large uncertainties, can be replaced by the actual values of the thrust and power coefficients measured experimentally by the manufacturer. Apart from uncertainty reduction, restricting the design to a fixed set of components reduces costs and improves development times, making it popular among designers in a variety of technical fields. However, it is rare that a system can be designed solely from off-the-shelf components. For example, an aircraft designer will not find a ready-made airframe on the market. Designers may also want to explore future technologies for which databases are not yet available, hence requiring analytical models. Therefore, there is a need for a design optimization methodology allowing sizing systems that combine both custom and off-the-shelf components. Such a hybrid approach benefits from the detailed description provided by datasheets and the ability of continuous design models to explore a greater design space.

### *5.1. Proposed methodology*

Figures 14, 15a and 15b provide an overview of the proposed hybrid design optimization with an extended design structure matrix (XDSM) diagram [47].

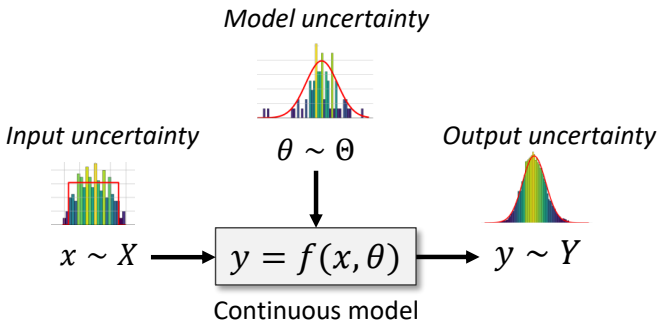


Figure 12: Custom component described with models.

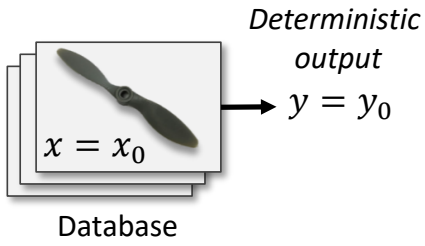


Figure 13: Existing component described with deterministic data.

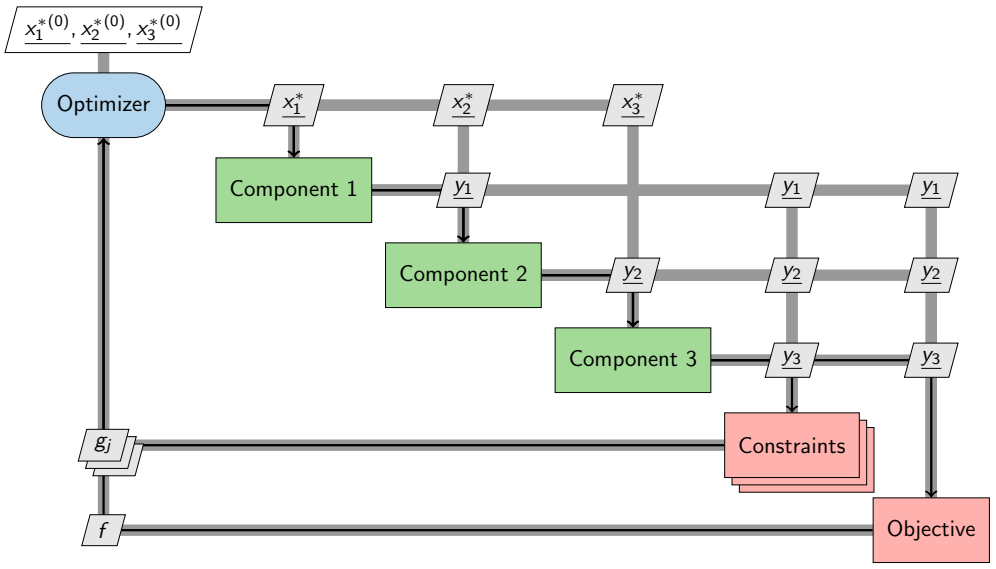


Figure 14: Extended design structure matrix diagram for the hybrid design optimization.

The design optimization problem is expressed as follows:

$$\begin{aligned} &\underset{\underline{x^*}}{\text{minimize}} \quad f(\underline{x^*}) \\ &\text{subject to} \quad g_j(\underline{x^*}) \leq 0,\ j = 1, \ldots, m. \end{aligned} \tag{19}$$

where $f$ is the objective function to be minimized (or maximized) by solving for the set of continuous design variables $\underline{x^*}$, and $g_j(\underline{x^*}) \leq 0$ are inequality constraints. The hybrid design optimization addresses this problem by solving the individual component analyses (depicted by green boxes in Figure 14) with either continuous models or discrete off-the-shelf selections without the need to reformulate the optimization problem.

When the designer is targeting a custom-made component or no database is available, a design model is used to return an estimate of the functional parameters and characteristics of the component based on the value of its design

variables. This sizing process is illustrated in Figure 15a, where the continuous design variables $\underline{x_i^*}$ and model parameters $\underline{\theta_i^*}$ may contain deviations from physical reality, as explained in Section 3. The illustration is simplified for clarity. For more complex problems, the outputs of the upstream component analyses can be used as inputs to the design model, adding to the propagation of uncertainty.

When a database with off-the-shelf components is available, the sizing of a component is a two-step process, illustrated in Figure 15b. First, the candidate component that most closely matches the values of the continuous design variables is selected. This translates the continuous design variables $\underline{x^*}$ into discrete variables $\underline{x}$ describing an existing component. The dependent parameters of the corresponding component are then extracted from its datasheet instead of being estimated with design models. This approach allows for removing both variable uncertainty and model uncertainty.

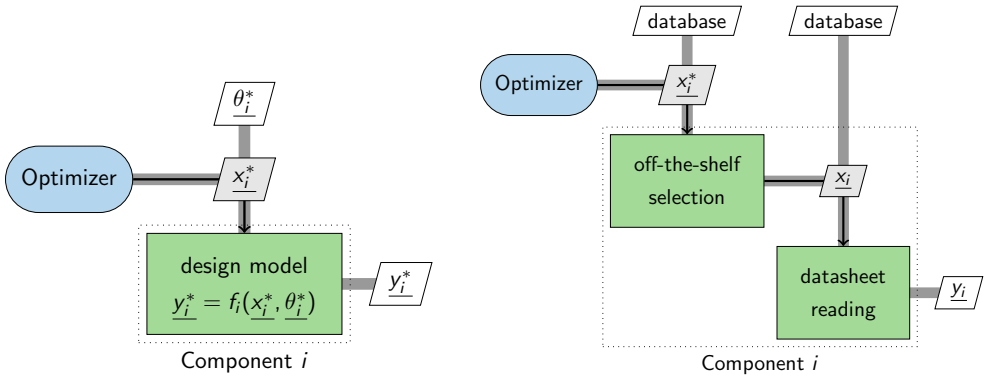


(a) Design model approach.

(b) Off-the-shelf selection approach.

Figure 15: Sizing process at component level.

The hybrid design optimization offers several advantages:

- The designer can define which components are selected from a database and which are custom-made by replacing the corresponding component analysis. A hybrid design combining both off-the-shelf components and custom-made components is therefore obtained.

- The formulation of the optimization problem remains the same as in a continuous design approach, with a reduced number of design variables. The choice regarding which method is used to size the components does not change the problem formulation, as the interfaces between the optimizer and the components are preserved. In addition, the bounds on the design variables are independent of the number of components stored in the databases.

- The nested analyses inherent to an MDO approach ensure that an optimal and consistent design is obtained. This is a significant advance compared to approaches where an optimization in the continuous space is followed by an offline selection of off-the-shelf components, which no longer guarantees optimality and compliance with optimization constraints as well as consistency of the multidisciplinary couplings.

The hybrid design optimization methodology proposed here offers a single, unique framework for both custom and off-the-shelf solutions. It can be derived from most continuous design methodologies in a minimally invasive way and requires no reformulation effort of the optimization problem.

*5.2. Good practices for an efficient off-the-shelf selection*

Selecting a component from a database can be done in many different ways, but not all will lead to the same result. It is, therefore, necessary to

adopt a methodological approach to perform this task.

First, appropriate design variables must be chosen for sizing and selecting the components. A common choice is to use sensitivity analysis to find the parameters that most influence the optimization problem. However, this approach does not provide information on the parameter correlations. Since the optimizer can vary each design variable independently, the physical parameters chosen as such must be uncorrelated for consistency. Furthermore, choosing uncorrelated parameters allows for discriminating more efficiently the components in a database and thus facilitates the selection process. Methods to assist in this analysis include correlation matrices or principal component analyses (PCA). Figure 16 shows a PCA applied to brushless motors. The explained variance, that is, the proportion of variation in the database that can be attributed to each of the principal components (eigenvectors) generated by the PCA method, is shown in Figure 16a. The first two principal components are found to explain 72% of the variance within the database. An orthonormal basis is constructed from these two principal components, and the main physical parameters of the motor are projected into this basis, as depicted in Figure 16b. The direction of the vectors representing the motor parameters shows little correlation between the nominal torque, the velocity constant, and the motor resistance. These three parameters can therefore be chosen as design variables. In practice, design variables are chosen to be representative of functional parameters rather than imperfections. Consequently, the resistance is discarded. Only two parameters, the nominal torque and the velocity constant are set up as design variables. The remaining parameters are defined as dependent parameters. The reduction

in the number of design variables reduces the complexity of the optimization problem, although it increases the risk of not being able to distinguish two candidate components in the database.

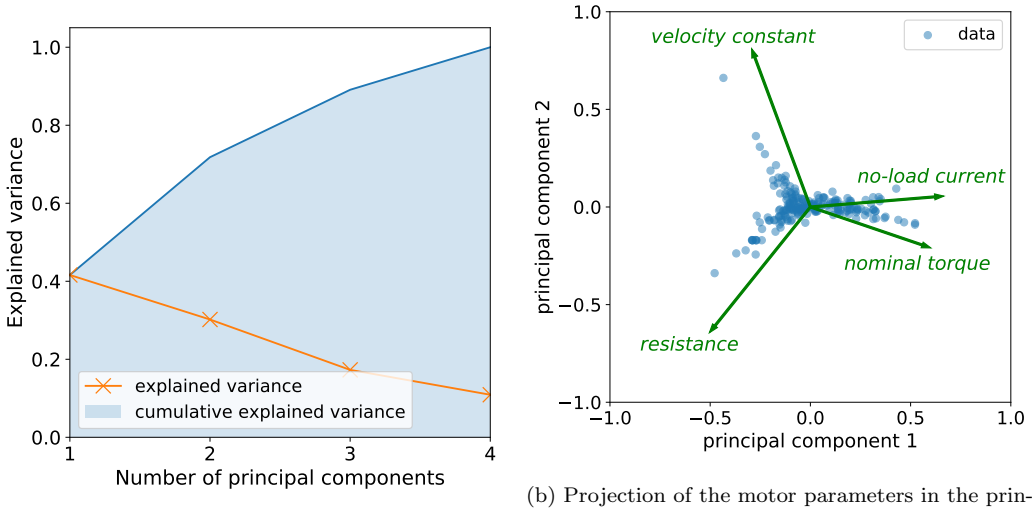


(a) Explained variance

(b) Projection of the motor parameters in the principal components basis.

Figure 16: Principal component analysis of the motor database [41, 48, 49].

Secondly, for off-the-shelf components, cleaning the database is a critical part of the methodological approach. Filtering the database reduces its dimension and thereby speeds up the selection process. It also allows removing components that have no interest in the application, in effect, components that do not correspond to an optimal solution of the design problem. Such restriction of the search space leads to better convergence properties. A Pareto analysis enables to narrow the database to a reduced set of efficient candidates. Figure 17 shows a torque versus weight plot for brushless motors. Pareto-efficient solutions with a high torque-to-weight ratio are highlighted in red. The other components are discarded, as they exhibit higher mass

penalties for similar mechanical performance. Particular attention must be given to this step, as excessive filtering can lead to sparse data coverage and bias the search for an optimal combination of components at the system level.

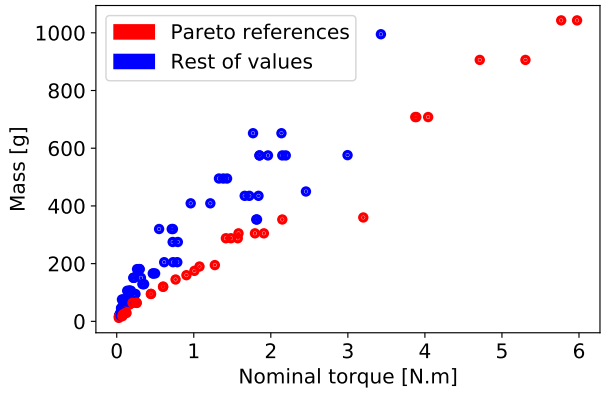


Figure 17: Pareto front for UAV motors [41, 48, 49].

Finally, a selection technique must be chosen. The problem of finding the candidate component in a database that is closest to a given set of design variables consists of a nearest neighbor search (NNS). It requires defining a distance metric based on which candidate solutions will be compared. The brute force method computes the distance from the given point to every other point in the database, and as such has a running time complexity of $\mathcal{O}(D \times N)$, where $D$ is the number of design variables and $N$ is the number of candidate components in the database. The search process can be sped up using space-partitioning methods such as ball tree or k-d tree, with a running time cost of approximately $\mathcal{O}(D \times \log(N))$ [50]. Lastly, normalization of the metric space is recommended. However, it can be desirable to bias the search in favor of one design variable by weighting the corresponding metric axis. Further work should help define a predominant design variable in the

selection process, for example, by analyzing the sensitivity of the optimization objective to each variable.

### *5.3. Optimization algorithm*

The design process presented in Section 5 contains discontinuities introduced by the discretization of the components design space in case off-the-shelf components are integrated. Therefore, the optimization problem is poorly suited to gradient-based optimizers. For their part, derivative-free optimization methods are more robust against ruggedness and local minima. Among them, the covariance matrix adaptation evolution strategy (CMA-ES) [51, 52] has proven to be successful in many applications with complex functions and requires minimal tuning. A Python implementation of CMA-ES is available in the *pycma* library [53].

### *5.4. Case study: design optimization of a multirotor UAV*

The hybrid design optimization is performed on the hexacopter drone introduced in Section 4.3, with the specifications provided in Table 4. The optimization problem consists of minimizing the total mass of the UAV. Various design variables describing the components (e.g., propeller geometry, motor nominal torque, battery energy) are initialized, and an initial mass is estimated with models or datasheets. The process is repeated with updated values until an optimal design that meets all requirements (e.g., hover endurance is greater than or equal to 18 min) is obtained. Three different designs are optimized and compared:

1. A completely custom design based on the models introduced in Section 3, Table 1.

2. A hybrid design made of custom components for the propulsion system, apart from the propeller, which is selected off-the-shelf to minimize the main source of uncertainty.
3. A design with off-the-shelf components for the propulsion system.

The off-the-shelf components used in the design optimization are taken from manufacturers' catalogs available online [2]. The main results and design variables representing the components are presented in Table 7. Figure 18 shows the mass distribution of the different UAV designs, and Figure 19 provides the flight endurance distributions. The custom propeller offers a slightly higher efficiency (higher $C_T/C_P$ ratio), which results in lower energy consumption for the same thrust. This is reflected in the battery energy and mass, which is minimal for the custom design. However, the off-the-shelf propellers are smaller, which allows for shorter arms, hence reducing the airframe's weight. Overall, excluding uncertainties, all three designs have similar mass and performance. In this particular case, the models and design variables used for the custom UAV proved to be particularly well-fitted to commercially available data, which explains the similarity of the results. However, in the absence of such information, the mass and the flight endurance hold very different uncertainties from one design to another. Due to input and model uncertainties, the custom design exhibits a standard deviation of 3.2 minutes for hover endurance. This translates to a 31% risk of having a flight endurance below 16.5 minutes instead of the specified 18

[2]Manufacturers' catalogs: APC [31], AXI [41, 54], Scorpion [48], KDE [49], Gens ACE [55], Tattu [56], Kokam [57], Thunder Power [42, 58], YGE [43], Turnigy [59], KOSMIK [60]

minutes. The probability decreases to 7% for the hybrid design and is null for the off-the-shelf design.

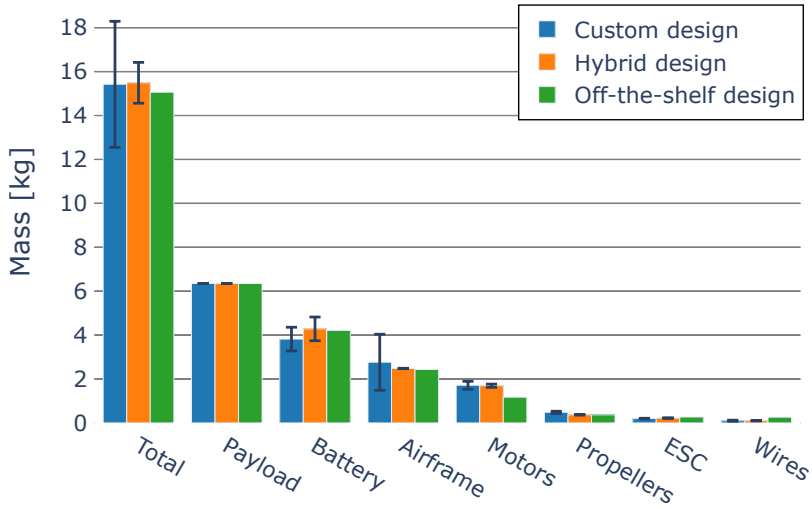


Figure 18: Mass distribution for the different UAV designs.

## 6. Conclusions

The present article introduces a new approach for quantifying and mitigating uncertainties in design optimization by addressing uncertainties related to both design models and off-the-shelf component availability. The contributions of the present methodology are twofold. First, it formalizes the uncertain availability of components in the market. Second, it enables the design optimization of systems with both custom and off-the-shelf components. In this process, a component is either described using continuous design variables and design models or using actual data provided by manufacturers, thereby reducing any related uncertainties.

Table 7: Optimization results of the different UAV designs.

| | 1. Custom design | 2. Hybrid design | 3. Off-the-shelf design |
|---|---|---|---|
| Propeller | Custom propeller | APC 18x5.5MR | APC 18x5.5MR |
| | $D = 0.489$ m, $\beta = 0.300$ | $D = 0.457$ m, $\beta = 0.306$ | $D = 0.457$ m, $\beta = 0.306$ |
| | $C_T = 0.0859$, $C_P = 0.0277$ | $C_T = 0.0839$, $C_P = 0.0284$ | $C_T = 0.0839$, $C_P = 0.0284$ |
| Motor | Custom motor | Custom motor | KDE 4215XF-465 |
| | $T_{nom} = 1.025$ N.m | $T_{nom} = 1.012$ N.m | $T_{nom} = 1.273$ N.m |
| | $K_V = 20.78$ rad/V/s | $K_V = 22.90$ rad/V/s | $K_V = 48.7$ rad/V/s |
| ESC | Custom ESC | Custom ESC | Jeti Spin 48 Opto |
| | $P = 890$ W, $U = 34$ V | $P = 992$ W, $U = 34.8$ V | $P = 1776$ W, $U = 37.0$ V |
| Battery | Custom battery | Custom battery | 36Ah 6S 25C LiPo[1] |
| | $E = 730$ Wh, $U = 34$ V | $E = 819$ Wh, $U = 34.8$ V | $E = 799$ Wh, $U = 22.2$ V |
| Total mass | $\mu = 15.4$ kg | $\mu = 15.5$ kg | $\mu = 15.1$ kg |
| | $\sigma = 1.4$ kg | $\sigma = 0.5$ kg | $\sigma = 0.0$ kg |
| Hover endurance | $\mu = 18.1$ min | $\mu = 18.0$ min | $\mu = 18.1$ min |
| | $\sigma = 3.2$ min | $\sigma = 1.0$ min | $\sigma = 0.0$ min |

[1] *6-P Thunder Power RC TP6000-6SPX25 or equivalent.*

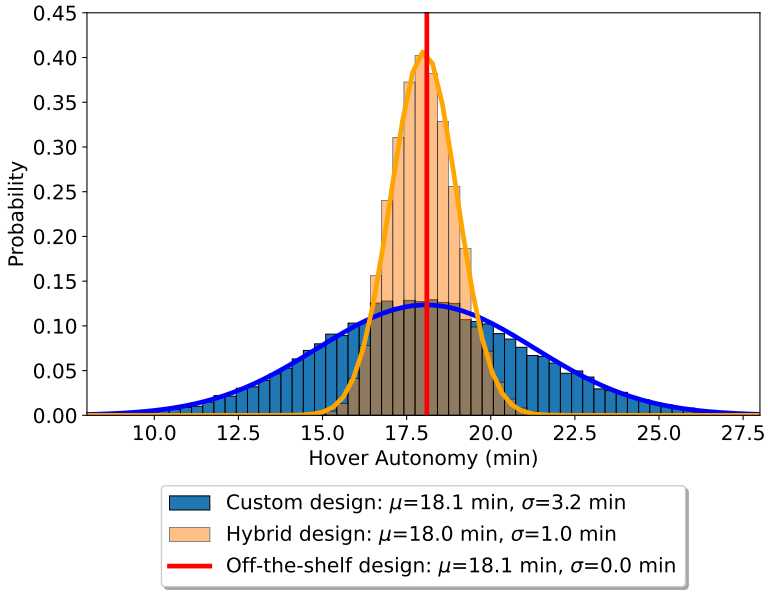


Figure 19: Distributions of the hover endurance estimation resulting from the custom, off-the-shelf, and hybrid design approaches.

To this end, the main sources of uncertainty in conceptual design are characterized. Input uncertainty, which refers to the unknown availability of a component in the market, is characterized by the distribution of the design variables' values within a size range. This distribution follows either an arithmetic or a geometric progression. Input uncertainty is then compared to model uncertainty arising from an inadequate structure of the design models or erroneous fitting of their parameters. Analytical criteria on components' distribution in the market allow evaluating the relative importance of input and model uncertainty with a first-order approximation. A more advanced analysis relies on numerical methods to propagate uncertainties through the system models and to rank the effects of different uncertain parameters on the output variation. Application to an electric multirotor UAV shows that

uncertainty in the aerodynamic model of the propeller is critical regarding hover flight endurance. In addition, the large number of components available in the UAV market makes input uncertainties of secondary importance.

Next, a methodology for uncertainty reduction in multidisciplinary design optimization is proposed. Uncertainty mitigation is achieved by replacing the design models with datasheets describing a specific component selected off-the-shelf. For this purpose, the methodology enables the design optimization of a system whose components are either parameterized with models or selected off-the-shelf. This is achieved by replacing the individual component analyses in the MDO process. Compared to state-of-the-art approaches, the design methodology introduced in this paper allows easy switching between custom and off-the-shelf components without having to reformulate the optimization problem. In addition, it returns a truly optimal design rather than mapping the analytical solution to the most proximate set of components. Good practices for improving the components' selection process are provided. The set of design variables best suited to the problem is obtained with a PCA, and the exploration of the component databases is improved by applying a Pareto filter. Finally, the relevance of this approach is demonstrated with a multirotor UAV case study. Three designs with different degrees of custom versus off-the-shelf components are optimized. The results show a significant reduction in performance uncertainty of 69% when the most critical component, namely the propeller, is off-the-shelf.

Further research should address the following limitations of the presented work. Input uncertainty as modelled in Section 3 assumes independent design variables, though it might not always be verified in practice. Identification of

a primary design variable, whose distribution follows arithmetic or geometric progression, and secondary design variables, whose distribution is weakly related to the primary variable, could refine the quantification of uncertainty. In design optimization, the influence of the design variable choices on the sizing results should be further investigated. For example, prioritization of one design variable over another in the discrete selection process should be investigated by analyzing the sensitivity of the final objective to each variable. With these improvements, the proposed methodology will provide a novel and effective means of quantifying and mitigating uncertainty in the design optimization of aerial vehicles.

**Funding Sources and Acknowledgments**

The presented work was funded by ISAE-SUPAERO, INSA Toulouse, and the Toulouse School of Aerospace Engineering through the French *Programme d'Investissements d'avenir* ANR-17-EURE-0005 conducted by ANR.

**Supplementary Materials**

Supplementary materials include the Jupyter Notebook and databases used to obtain the results on input uncertainty shown in Section 3, Figures 5 and 8.

## Appendix A. Uncertain parameters for the case study

Table A.8: Assumptions on uncertain parameters.

| Name | Type of uncertainty | Nominal value | Error distribution |
|---|---|---|---|
| Propeller diameter (m) | Input | 0.489 | $\mathcal{U}(-0.013, 0.013)$ |
| Propeller pitch-to-diameter ratio (-) | Input | 0.30 | $\mathcal{U}(-0.01, 0.01)$ |
| Propeller mass (kg) | Model | 0.080 | $\mathcal{N}(0, 10.0\%)$ |
| Propeller coefficient $C_T$ (-) | Model | 0.0859 | $\mathcal{N}(0, 8.8\%)$ |
| Propeller coefficient $C_P$ (-) | Model | 0.0277 | $\mathcal{N}(0, 7.5\%)$ |
| Motor velocity constant (rad/V/s) | Input | 20.78 | $\mathcal{U}(-3.5\%, 3.5\%)$ |
| Motor nominal torque (N.m) | Input | 1.025 | $\mathcal{U}(-4.9\%, 4.9\%)$ |
| Motor mass (kg) | Model | 0.285 | $\mathcal{N}(0, 11.5\%)$ |
| Motor resistance (V/A) | Model | 0.248 | $\mathcal{N}(0, 13.2\%)$ |
| Motor friction torque (N.m) | Model | 0.0149 | $\mathcal{N}(0, 33.4\%)$ |
| Battery energy (Wh) | Input | 730 | $\mathcal{U}(-5, 5)$ |
| Battery mass (kg) | Model | 3.82 | $\mathcal{N}(0, 7.1\%)$ |
| ESC power (W) | Input | 890 | $\mathcal{U}(-294, 294)$ |
| ESC mass (kg) | Model | 0.0329 | $\mathcal{N}(0, 25.4\%)$ |
| ESC efficiency (-) | Expert judgment | 0.95 | $\mathcal{U}(-0.05, 0.05)$ |

*Values are based on manufacturers' catalogs [31, 41, 42, 43], and Budinger [29].*

## References


[1] A. Papageorgiou, M. Tarkian, K. Amadori, J. Ölvander, Multidisciplinary Design Optimization of Aerial Vehicles: A Review of Recent Advancements (2018). doi:10.1155/2018/4258020.

[2] C. David, S. Delbecq, S. Defoort, P. Schmollgruber, E. Benard, V. Pommier-Budinger, From FAST to FAST-OAD: An open source framework for rapid Overall Aircraft Design, IOP Conference Series Materials Science and Engineering 1024 (2021) 012062. doi:10.1088/1757-899X/1024/1/012062.

[3] F. Lutz, J. Jézégou, A. Reysset, A. Busteros Ramos, V. Pommier-Budinger, FAST-OAD-GA: an open-source extension for Overall Aircraft Design of General Aviation aircraft, in: ICAS 2022, Stockholm, Sweden, 2022.
URL https://hal.archives-ouvertes.fr/hal-03828230

[4] S. Delbecq, M. Budinger, A. Ochotorena, A. Reysset, F. Defay, Efficient sizing and optimization of multirotor drones based on scaling laws and similarity models, Aerospace Science and Technology 102 (2020) 105873. doi:10.1016/j.ast.2020.105873.
URL https://linkinghub.elsevier.com/retrieve/pii/S1270963820305551

[5] K. Fayez, Y. Leng, T. Jardin, M. Bronz, J.-M. Moschetta, Conceptual Design for Long-Endurance Convertible Unmanned Aerial System, in: AIAA Scitech 2021 Forum, AIAA SciTech Forum, American Institute

of Aeronautics and Astronautics, 2021. doi:10.2514/6.2021-1059.
URL https://arc.aiaa.org/doi/10.2514/6.2021-1059

[6] D. Lim, H. Kim, K. Yee, Mission-oriented performance assessment and optimization of electric multirotors, Aerospace Science and Technology 115 (2021) 106773. doi:10.1016/j.ast.2021.106773.
URL https://www.sciencedirect.com/science/article/pii/S1270963821002832

[7] D. Bershadsky, S. Haviland, E. N. Johnson, Electric Multirotor UAV Propulsion System Sizing for Performance Prediction and Design Optimization, in: 57th AIAA/ASCE/AHS/ASC Structures, Structural Dynamics, and Materials Conference, American Institute of Aeronautics and Astronautics, San Diego, California, USA, 2016. doi:10.2514/6.2016-0581.
URL https://arc.aiaa.org/doi/10.2514/6.2016-0581

[8] M. J. Daskilewicz, B. J. German, T. T. Takahashi, S. Donovan, A. Shajanian, Effects of disciplinary uncertainty on multi-objective optimization in aircraft conceptual design, Structural and Multidisciplinary Optimization 44 (6) (2011) 831–846. doi:10.1007/s00158-011-0673-4.
URL https://doi.org/10.1007/s00158-011-0673-4

[9] L. Jaeger, C. Gogu, S. Segonds, C. Bes, Aircraft Multidisciplinary Design Optimization Under Both Model and Design Variables Uncertainty, Journal of Aircraft 50 (2) (2013) 528–538, publisher: American Institute of Aeronautics and Astronautics. doi:10.2514/1.C031914.
URL https://arc.aiaa.org/doi/10.2514/1.C031914

[10] Y. Deremaux, N. Pietremont, J. Negrier, E. Herbin, M. Ravachol, Environmental MDO and uncertainty hybrid approach applied to a supersonic business jet, in: 12th AIAA/ISSMO multidisciplinary analysis and optimization conference, 2008, p. 5832.

[11] D. Lim, H. Kim, K. Yee, Uncertainty propagation in flight performance of multirotor with parametric and model uncertainties, Aerospace Science and Technology (2022) 107398doi:10.1016/j.ast.2022.107398.
URL https://www.sciencedirect.com/science/article/pii/S1270963822000724

[12] D. Neufeld, J. Chung, K. Behdinian, Aircraft Conceptual Design Optimization Considering Fidelity Uncertainties, Journal of Aircraft 48 (5) (2011) 1602–1612. doi:10.2514/1.C031312.
URL https://arc.aiaa.org/doi/10.2514/1.C031312

[13] N. Smith, S. Mahadevan, Probabilistic Methods for Aerospace System Conceptual Design, Journal of Spacecraft and Rockets 40 (3) (2003) 411–418, publisher: American Institute of Aeronautics and Astronautics. doi:10.2514/2.3961.
URL https://arc.aiaa.org/doi/10.2514/2.3961

[14] J. Zhang, H. Tang, M. Chen, Robust design of an adaptive cycle engine performance under component performance uncertainty, Aerospace Science and Technology 113 (2021) 106704. doi:https://doi.org/10.1016/j.ast.2021.106704.

[15] F. Fusi, P. M. Congedo, A. Guardone, G. Quaranta, Assessment of

robust optimization for design of rotorcraft airfoils in forward flight, Aerospace Science and Technology 107 (2020) 106355. doi:https://doi.org/10.1016/j.ast.2020.106355.

[16] M. Biczyski, R. Sehab, J. F. Whidborne, G. Krebs, P. Luk, Multirotor Sizing Methodology with Flight Time Estimation, Journal of Advanced Transportation 2020 (2020) e9689604, publisher: Hindawi. doi:10.1155/2020/9689604.
URL https://www.hindawi.com/journals/jat/2020/9689604/

[17] O. Magnussen, G. Hovland, M. Ottestad, Multicopter UAV design optimization, in: 2014 IEEE/ASME 10th International Conference on Mechatronic and Embedded Systems and Applications (MESA), 2014, pp. 1–6. doi:10.1109/MESA.2014.6935598.

[18] O. Magnussen, M. Ottestad, G. Hovland, Multicopter Design Optimization and Validation, Modeling, Identification and Control: A Norwegian Research Bulletin 36 (2) (2015) 67–79. doi:10.4173/mic.2015.2.1.
URL http://www.mic-journal.no/ABS/MIC-2015-2-1.asp

[19] W. Pawlus, G. Hovland, M. Choux, D. Frick, M. Morari, Drivetrain design optimization for electrically actuated systems via mixed integer programing, 2015, pages: 001470. doi:10.1109/IECON.2015.7392307.

[20] T. T. H. Ng, G. S. B. Leng, Design of small-scale quadrotor unmanned air vehicles using genetic algorithms, Proceedings of the Institution of Mechanical Engineers, Part G: Journal of Aerospace Engineering 221 (5) (2007) 893–905, publisher: IMECHE. doi:10.1243/

09544100JAERO113.
URL https://doi.org/10.1243/09544100JAERO113

[21] V. M. Arellano-Quintana, E. A. Portilla-Flores, E. A. Merchan-Cruz, P. A. Niño-Suarez, Multirotor design optimization using a genetic algorithm, in: 2016 International Conference on Unmanned Aircraft Systems (ICUAS), 2016, pp. 1313–1318. doi:10.1109/ICUAS.2016.7502564.

[22] P. M. Renkert, A. G. Alleyne, Component-Based Design Optimization of Multirotor Aircraft, in: 2022 American Control Conference (ACC), 2022, pp. 3985–3990, iSSN: 2378-5861. doi:10.23919/ACC53348.2022.9867163.

[23] S. Oh, M. Kim, H. Kim, D. Lim, K. Yee, D. Kim, The Solution Development for Performance Analysis and Optimal Design of Multicopter-type Small Drones, in: 2020 International Conference on Unmanned Aircraft Systems (ICUAS), 2020, pp. 975–982, iSSN: 2575-7296. doi:10.1109/ICUAS48674.2020.9213985.

[24] P. Saves, E. Nguyen Van, N. Bartoli, T. Lefebvre, C. David, S. Defoort, Y. Diouane, J. Morlier, Bayesian optimization for mixed variables using an adaptive dimension reduction process: applications to aircraft design, in: AIAA SciTech 2022, San Diego, United States, 2022. doi:10.2514/6.2022-0082.
URL https://hal.archives-ouvertes.fr/hal-03514915

[25] M. Lemaire, Approche probabiliste du dimensionnement - Modélisation de l'incertain et méthode de Monte-Carlo (2014) 21.

[26] Lemaire Maurice, Mécanique et incertain / Maurice Lemaire, Collection Génie mécanique et mécanique des solides, ISTE editions, London, 2014.

[27] C. Gogu, Ingénierie mécanique en contexte incertain: Des approches classiques à quelques développements récents, Encyclopédie SCIENCES, Iste editions., 2021.
URL https://books.google.fr/books?id=zTMQEAAAQBAJ

[28] E. de Rocquigny, N. Devictor, S. Tarantola (Eds.), Uncertainty in Industrial Practice, John Wiley & Sons, Ltd, Chichester, UK, 2008. doi:10.1002/9780470770733.
URL http://doi.wiley.com/10.1002/9780470770733

[29] M. Budinger, A. Reysset, A. Ochotorena, S. Delbecq, Scaling laws and similarity models for the preliminary design of multirotor drones, Aerospace Science and Technology 98 (2020) 105658. doi:10.1016/j.ast.2019.105658.
URL https://linkinghub.elsevier.com/retrieve/pii/S1270963819321686

[30] G. Pahl, W. Beitz, J. Feldhusen, K.-H. Grote, Engineering Design: A Systematic Approach, 3rd Edition, Springer-Verlag, London, 2007. doi:10.1007/978-1-84628-319-2.
URL https://www.springer.com/gp/book/9781846283185

[31] APC Propellers.
URL https://www.apcprop.com/shop/?product_cat=multi-rotor-electric-only

[32] ABB Motors.
URL https://new.abb.com/motors-generators/iec-low-voltage-motors

[33] I. Sobol, Sensitivity Estimates for Nonlinear Mathematical Models, undefined (1993).
URL https://www.semanticscholar.org/paper/Sensitivity-Estimates-for-Nonlinear-Mathematical-Sobol/3e0b415213a580254226fdbcbfc9980b70dd0468

[34] I. M. Sobol, Global sensitivity indices for nonlinear mathematical models and their Monte Carlo estimates, Mathematics and Computers in Simulation 55 (1) (2001) 271–280. doi:10.1016/S0378-4754(00)00270-6.
URL https://www.sciencedirect.com/science/article/pii/S0378475400002706

[35] T. Homma, A. Saltelli, Importance measures in global sensitivity analysis of nonlinear models, Reliability Engineering & System Safety 52 (1) (1996) 1–17. doi:10.1016/0951-8320(96)00002-6.
URL https://www.sciencedirect.com/science/article/pii/0951832096000026

[36] M. D. Morris, Factorial Sampling Plans for Preliminary Computational Experiments, Technometrics 33 (2) (1991) 161–174, publisher: Taylor & Francis _eprint: https://www.tandfonline.com/doi/pdf/10.1080/00401706.1991.10484804. doi:10.1080/00401706.1991.10484804.

URL https://www.tandfonline.com/doi/abs/10.1080/00401706.1991.10484804

[37] A. Saltelli, S. Tarantola, F. Campolongo, M. Ratto, Sensitivity Analysis in Practice, John Wiley & Sons, Ltd, Chichester, UK, 2002. doi:10.1002/0470870958.
URL http://doi.wiley.com/10.1002/0470870958

[38] DJI M600 Pro.
URL https://www.dji.com/matrice600-pro

[39] F. Pollet, S. Delbecq, M. Budinger, J.-M. Moschetta, Design optimization of multirotor drones in forward flight, in: 32nd Congress of the International Council of the Aeronautical Sciences, 2021.

[40] F. Pollet, S. Delbecq, M. Budinger, J.-M. Moschetta, J. Liscouët, A common framework for the design optimization of fixed-wing, multicopter and VTOL UAV configurations, in: 33rd Congress of the International Council of the Aeronautical Sciences, Stockholm, Sweden, 2022.
URL https://hal.archives-ouvertes.fr/hal-03832115

[41] AXI Model Motors.
URL https://www.modelmotors.cz/

[42] Thunder Power ProLiteX.
URL https://www.thunderpowerrc.com/collections/prolitex-series-25c

[43] YGE ESC.
URL https://www.yge.de/en/home-2/

[44] T. Kluyver, B. Ragan-Kelley, F. Perez, B. Granger, M. Bussonnier, J. Frederic, K. Kelley, J. Hamrick, J. Grout, S. Corlay, P. Ivanov, D. Avila, S. Abdalla, C. Willing, J. [Unknown, Jupyter Notebooks – a publishing format for reproducible computational workflows, 2016.

[45] M. Baudin, A. Dutfoy, B. Iooss, A.-L. Popelin, OpenTURNS: An Industrial Software for Uncertainty Quantification in Simulation, Springer International Publishing, Cham, 2016, pp. 1–38. doi:10.1007/978-3-319-11259-6_64-1.
URL https://doi.org/10.1007/978-3-319-11259-6_64-1

[46] J. Herman, W. Usher, SALib: An open-source python library for sensitivity analysis, The Journal of Open Source Software 2 (9) (jan 2017). doi:10.21105/joss.00097.
URL https://doi.org/10.21105/joss.00097

[47] A. B. Lambe, J. R. R. A. Martins, Extensions to the design structure matrix for the description of multidisciplinary design, analysis, and optimization processes, Structural and Multidisciplinary Optimization 46 (2) (2012) 273–284. doi:10.1007/s00158-012-0763-y.
URL https://doi.org/10.1007/s00158-012-0763-y

[48] Scorpion Motors.
URL https://www.scorpionsystem.com/catalog/helicopter/motors_4/

[49] KDE Direct.
URL https://www.scorpionsystem.com/catalog/aeroplane/

[50] Scikit Learn Neighbors.
URL https://scikit-learn.org/stable/modules/neighbors.html

[51] N. Hansen, A. Ostermeier, Adapting arbitrary normal mutation distributions in evolution strategies: The covariance matrix adaptation, 1996, journal Abbreviation: Proceedings of the IEEE Conference on Evolutionary Computation Pages: 317 Publication Title: Proceedings of the IEEE Conference on Evolutionary Computation. doi:10.1109/ICEC.1996.542381.

[52] A. Auger, N. Hansen, Tutorial CMA-ES — Evolution Strategies and Covariance Matrix Adaptation 83.

[53] N. Hansen, yoshihikoueno, ARF1, K. Nozawa, M. Chan, Y. Akimoto, D. Brockhoff, CMA-ES/pycma: r3.1.0 (Jun. 2021). doi:10.5281/zenodo.5002422.
URL https://zenodo.org/record/5002422

[54] SPIN OPTO ESC.
URL https://www.modelmotors.cz/product/jeti-spin/

[55] Gens ACE.
URL https://www.gensace.de/

[56] Tattu.
URL https://www.genstattu.com/

[57] Kokam.
URL https://kokam.com/

[58] Thunder Power RAMPAGE.
URL https://www.thunderpowerrc.com/collections/rampage-high-discharge-series

[59] Turnigy.
URL https://turnigy.com/

[60] KOSMIK ESC.
URL https://www.kontronik.com/en/products/speedcontroller/speedcontroller1/kosmik.html